Takayama and Hisamatsu *Robomech J* (2019) 6:21
https://doi.org/10.1186/s40648-019-0149-7

ROBOMECH Journal

RESEARCH ARTICLE

Open Access

Worm gear mechanism with switchable backdrivability

Toshio Takayama* and Naoto Hisamatsu

Abstract

A worm gear has the advantages of a large reduction ratio and non-backdrivability. Because of this non-backdrivability, it can maintain a joint angle without energy consumption. Today, many robots have large workspaces that extend into the living spaces of humans, and they are required to work cooperatively with humans. In such cases, backdrivability is necessary to achieve high compliance for robots. Compliance helps robots perform cooperative tasks with humans, and protects its mechanisms and humans in the case of a collision. However, a worm gear cannot be backdriven because of the friction between tooth surfaces. Therefore, we have developed a worm gear mechanism that can switch its backdrivability using vibration that reduces friction. In this paper, we present a dynamic model of the worm gear to analyze the friction-reduction phenomenon caused by vibrations. We discuss the change in the effectiveness of the backdrivability with the change in the vibration direction. Finally, we experimentally confirm the certainty of the analysis.

Keywords: Worm gear, Backdrivability, Vibration

Introduction

Recently, robots with increased workspaces have been developed, and these robots work in the vicinity of (and together with) humans. Such robots are required to have high compliance for its joints, to avoid unexpected collisions [1]. Moreover, to perform tasks cooperatively with humans, a high compliance is essential for the robots. To perform compliance control, backdrivable mechanisms are typically used and the electric current of the motor is controlled. Some studies insist that electrical control lacks reliability. To achieve better human safety, a study developed a velocity- and contact force-based mechanical safety device [2]. Some studies introduced elastic elements between the actuator and the output joint to achieve better compliance [3]. Pneumatic actuators are also used for improving the compliance of the mechanism [4]. Moreover, soft robotics, in which the whole body of a robot is made from soft materials, is widely studied [5].

A worm gear has the advantages of a large reduction ratio and being able to hold the output position without energy consumption because of its non-backdrivability [6]. However, mechanisms that use a worm gear do not have compliance, because a worm gear does not have backdrivability. Moreover, because of the non-backdrivability of the worm gear, it requires complicated control methods [7, 8]. If a worm gear that can switch its backdrivability is developed, it can be used for a robot that requires compliance. We have utilized the non-backdrivability of the worm gear to develop some high-speed/high-torque coexistence devices [9, 10]. If such a backdrivability switchable worm gear were created, we could achieve high compliance on our high-speed/high-torque coexistence devices.

To provide the worm gear with backdrivability, a technique that uses a feedback control based on the measured torque was proposed [11]. However, if back-drivability is provided mechanically, the response and the reliability can be enhanced. Due to the friction between the teeth of the worm screw and the worm wheel, a worm gear cannot be backdriven. A worm gear-like mechanism that introduced rotatable gear teeth to the worm wheel

*Correspondence: takayama.t.aa@m.titech.ac.jp
Tokyo Institute of Technology, 2-12-1(I3-13) Ookayama, Meguro-ku, Tokyo 152-8552, Japan

was developed [12], where the mechanism could be backdriven mechanically but lost the advantage of non-backdrivability. Moreover, the proposed mechanism was composed of too many parts, which made it expensive for practical use. Therefore, we applied the friction reduction phenomenon by the vibrations [13, 14] to the worm gear. The developed worm gear can switch backdrivability appropriately, and it realized the sensorless high compliance worm gear [15, 16]. In this study, we created a dynamic model of the worm gear, analyzed the friction-reduction phenomenon caused by the vibration, and estimated vibration strength required to obtain backdrivability. Of course, the transmission efficiency is an important factor for a gear mechanism. If the efficiency was considered, we would also need to consider the energy required to generate the vibration and the structural design that had a resonance frequency to vibrate effectively. However, we considered that the proposed mechanism was typically used as a traditional worm gear to utilize its advantage of non-backdrivability, and created backdrivability when needed by applying vibration. In such a case, the term that the vibration was applied was limited, and the transmission efficiency became less important. Therefore, in this paper, we focus on the estimation of the vibration force and the frequency at which the worm gear can obtain backdrivability. Moreover, the difference in the effectiveness of the phenomenon with the difference in the vibration direction is discussed and quantitatively confirmed by the experiment.

The remainder of this paper is organized as follows; "Modeling method of the vibrating worm gear" section discusses the modeling method of the vibrating worm gear, "Theoretical difference of the backdrivability by the vibration direction" section presents the theoretical difference of the backdrivability by the vibration direction, "Experiment" section presents the experimental setup and experimental results, and finally "Discussion and conclusion" section discusses the experimental results and provides conclusions.

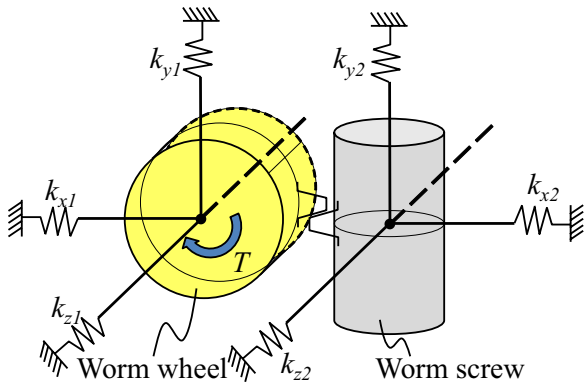

Fig. 1 Vibration model of the worm gear mechanism

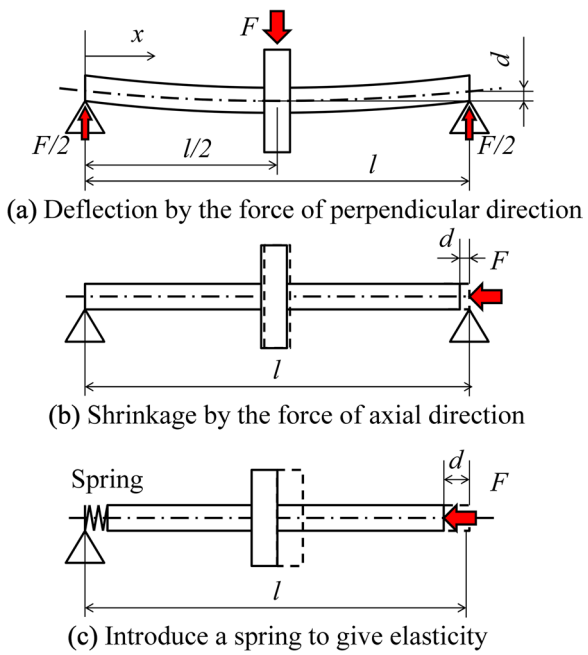

Fig. 2 Bending and shrinkage models of the shaft of the worm gear

Modeling method of the vibrating worm gear

We assume that the worm gear is a simple 6-DOF vibration model, shown in Fig. 1, to estimate the condition that gives backdrivability to the worm gear. The spring stiffnesses k_x1, k_y1, k_x2, and k_z2 are perpendicular to the axes of the worm wheel and the worm screw. They are assumed to be the stiffness of the simply supported beam as shown in Fig. 2a. k_z1 and k_y2 are the spring stiffnesses in the axial directions of the worm wheel and the worm screw, respectively. If the spring stiffness is assumed to be the stiffness of the compressed shaft, as shown in Fig. 2b, the spring stiffness becomes too large; thus, we introduce an additional spring, as shown in Fig. 2c.

The spring stiffness perpendicular to the axis can be calculated from the displacement of the axis when a force is applied at the center of the axis. Let F, $F/2$, E, I, A, and δ be the given force at the center of the axis, reaction force at both ends of the axis, Young's modulus, second moment of area, the cross-sectional area, and displacement, respectively. If the length from the end of the axis to the arbitrary point X is defined as x, the bending moment due to the reaction force about the center of the axis would be $M_{(x)} = Fx/2$. Using $M_{(x)}$ in the elastic curve equation produces Eq. (1). Integrating Eq. (1) and using the boundary condition $\delta_{(0)} = \delta_{(l)} = 0$ and $d\delta_{(l/2)}/dx = 0$, $\delta_{(x)}$ is obtained (2).

$$\frac{d^2\delta}{dx^2} = -\frac{M}{EI} = -\frac{Fx}{2EI} \tag{1}$$

$$\delta_{(x)} = \frac{F}{4EI}\left(-\frac{x^3}{3} + \frac{l^2 x}{4}\right) \tag{2}$$

Substituting $x = l/2$ in Eq. (2) results in $\delta_{(l/2)}$; spring stiffness of the axis $K_P = F/\delta_{(l/2)}$ is also obtained.

$$\delta_{(l/2)} = \frac{Fl^3}{48EI} \tag{3}$$

$$K_P = \frac{F}{\delta_{(l/2)}} = \frac{48EI}{l^3} \tag{4}$$

Spring stiffness in the axial direction (which is defined by the spring) is shown in Fig. 2c.

Theoretical difference of the backdrivability by the vibration direction

In this study, we used vibrations to achieve friction reduction in the worm gear. There are two types of friction reduction phenomena. The first type is caused by the jumping of the tooth surface of the worm gear by the vibration, which generates periodic conditions of contact and non-contact, and during the non-contact condition, it loses friction. The second type is caused by the vibration (oriented parallel to the lead angle), which exceeds the friction force. In the article [15] the bearings that hold the shafts of the worm gear are held by the rubber parts, and the shafts can vibrate in all directions. However, the vibration that changes the length between the shafts of the worm screw and the worm wheel is not recommended, because it significantly displaces the contact point from the pitch circle of the gear. Moreover, such motion causes a misalignment of the axes of the shafts. Therefore, in this paper we will discuss the vibrations caused in the direction of the axis of the worm screw and of the worm wheel [16], as such vibrations do not cause a change in the gap of the gear shafts.

The specifications of the worm gear (composed of a worm screw and a worm wheel) are shown in Table 1. We assembled the worm gear, and a pulley was installed to the shafts of both the worm screw and the worm wheel. First, a weight was hung on the pulley of the worm wheel to generate a contact force between the worm gear teeth. Next, the mass of the weight hung from the worm screw was increased slowly, and the weight initiated rotation of the worm gear was measured. Accordingly, we obtained the coefficient of static friction μ shown in Table 1.

Vibration in the direction of the worm screw axis

We consider the vibration that acts on the axis of the worm screw S_y, as shown in Fig. 3a. The weight of the

Table 1 Specification of the worm screw and wheel

	Number of thread	Number of teeth	Reference diameter (mm)	Weight (g)
Worm screw	2	–	16	42.0
Worm wheel	–	20	20	32.0
	Module	**Lead angle (°)**	**Normal pressure angle (°)**	μ
	1	7.18	20	0.175

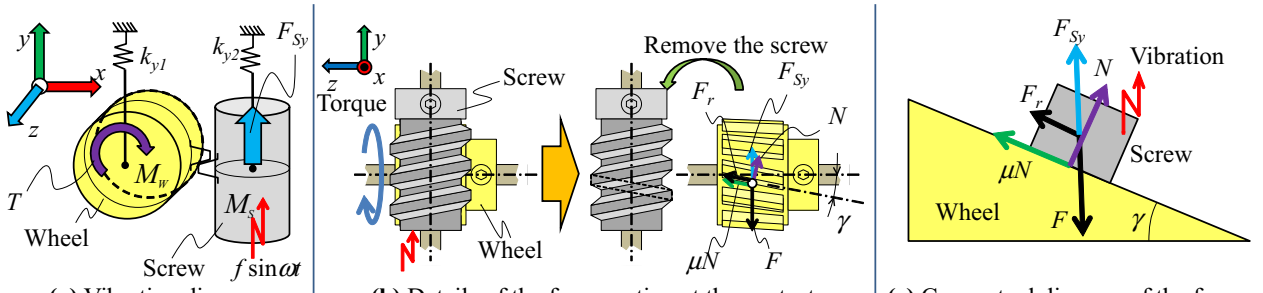

(a) Vibration diagram of the worm gear

(b) Details of the forces acting at the contact point of the worm wheel and the worm screw.

(c) Conceptual diagram of the forces between the teeth of the worm gear.

Fig. 3 Vibration to the screw-axis direction

worm wheel, the worm screw, and the exciting force are M_W, M_S, and $f \sin \omega t$, respectively. Theoretically, the x and z components of the force are also generated by the contact force of the gear teeth. However, they are smaller than y components of the force, because the lead angle of the worm gear is small. To simplify the analysis, we considered only the spring stiffness k_{y1} and k_{y2}. If the worm wheel and the worm screw are in contact in the static friction condition, they vibrate as a single body by the shaft of the worm wheel, bending by the motion shown in Fig. 2a. Therefore, the equation of the motion can be written as shown in Eq. (5), and the displacement y can be calculated.

$$(M_W + M_S)y'' + (k_{y1} + k_{y2})y = f \sin \omega t \tag{5}$$

The exciting force $f \sin \omega t$ and the restoring force of spring stiffness k_{y2} are applied to the worm screw. From Eq. (5), the force F_{Sy} that is applied to the y axis of the worm screw by the vibration, except for the force that is applied from the worm wheel via the gear tooth, can be calculated as follows.

$$F_{Sy} = -k_{y2}y + f \sin \omega t \tag{6}$$

This F_{Sy} becomes an applied force to the contact point by the worm screw.

We now consider the forces generated between the teeth of the worm wheel and the worm screw. The tooth surface is inclined by the lead angle and the pressure angle. To simplify the analysis, we consider only the lead angle γ, which has a significant effect on the friction of the teeth. Figure 3b shows the worm gear observed along the x axis. Another figure that removes the worm screw so that the contact point of the teeth can be seen is also shown. If torque is applied to the worm wheel shaft, a pushing force F is generated on the gear teeth via the worm wheel. This F becomes an applied force to the contact point by the worm wheel. Therefore, the contact point of the gear tooth is applied both forces of F_{Sy} and F.

Moreover, the worm screw can rotate around its axis, thus, if the amplitude of the vibration is small, the motion of the contact point can be considered as the motion on the yz plane. If we fix the coordinate system to the worm wheel, F relatively behaves as a force that is applied to the worm screw in the opposite direction. Therefore, the worm screw can be treated as an object on which a force of F acts while it rests against a surface inclined at γ, as shown in Fig. 3c. Of course, F includes both forces generated by spring k_y1 and the torque applied to the worm wheel. However, if the amplitude of the vibration is small, F is dominated by the force generated by torque T rather than the force generated by spring k_y1. Therefore, we assume F as constant to simplify the equation. By this simplification, F can be treated similar to a force generated by the gravitational acceleration, as shown in Fig. 3c. Because the pressing force caused by the vibration applied via the worm screw is F_{Sy}, the normal force N of the gear tooth surface is obtained as follows:

$$N = (F - F_{Sy}) \cos(\gamma) \tag{7}$$

Here, when $N = 0$, the teeth are in the non-contact condition, which means the teeth are on the verge of losing contact and begin to jump. We define Λ as $\Lambda = F_{Sy}/F$. Therefore, if $\Lambda = 1$ the teeth begin to jump.

Next, we consider the force F_r that is parallel to the inclined surface and obtain the condition in which the gear teeth begin to slip. Let the coefficient of friction be μ; F_r that is calculated as follows.

$$F_r = (F - F_{Sy}) \sin \gamma - \mu N \tag{8}$$

$$= (F - F_{Sy})(\sin \gamma - \mu \cos \gamma). \tag{9}$$

Figure 3 shows the condition in which the worm screw and the worm wheel move in unison without slippage. Therefore, $(F - F_{Sy}) \sin \gamma < \mu N$, $F_r < 0$, and the arrow representing F_r is in the negative direction.

Here, we define $\Lambda_r = F_r/F$.

$$\Lambda_r = (1 - \Lambda)(\sin \gamma - \mu \cos \gamma) \tag{10}$$

Therefore, in case of $\Lambda_r = 0$, the teeth of the worm gear begin to slip. This means that when $\Lambda = 1$ that is the same as the condition the worm gear starts jumping. Therefore, in this case, the teeth begin to jump at the same time that they begin to slip. According to the above results, when the force F_{Sy} is applied by the vibration to make $\Lambda > 1$, the gear teeth begin to jump and lose contact periodically; thus, there will be a decrease in friction force, and backdrivability is expected.

Vibration in the direction of the worm wheel axis

We consider the exciting force $f \sin \omega t$ that is applied to the axis of the worm wheel W_z, as shown in Fig. 4a. Similar to Eq. (5), if the worm wheel and the worm screw are in contact in the static friction condition, they vibrate as a single body. The equation of motion can be described as shown in Eq. (11), and the displacement z can be calculated.

$$(M_W + M_S)z'' + (k_{z1} + k_{z2})z = f \sin \omega t \tag{11}$$

The force generated between the gear teeth is shown in Fig. 4b, c. In this case, the worm wheel is placed on the inclined surface representing the worm screw and vibrated in the horizontal direction. The exciting force

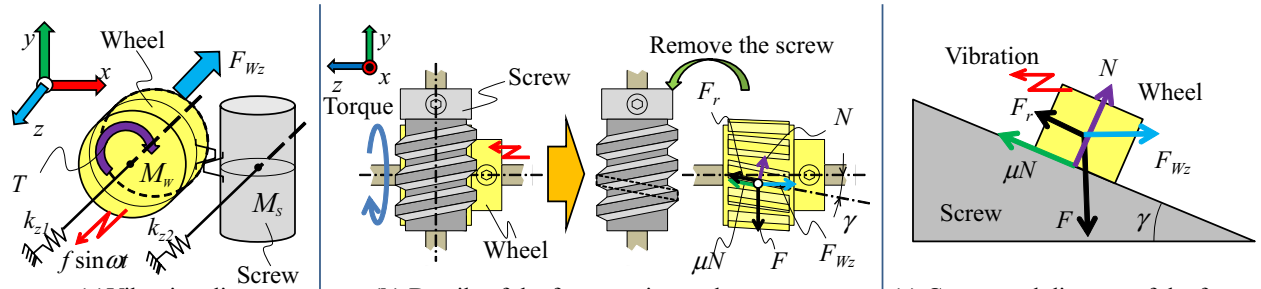

(a) Vibration diagram of the worm gear

(b) Details of the forces acting at the contact point of the worm wheel and the worm screw.

(c) Conceptual diagram of the forces between the teeth of the worm gear.

Fig. 4 Vibration to the wheel-axis direction

$f \sin \omega t$, the restoring force due to the spring constant k_{z1}, and the z element of the friction force $\mu N \cos \gamma$ act on the worm wheel. The applied force to the worm wheel in the z direction F_{Wz}, except for the force applied from the gear teeth, is calculated as follows;

$$F_{Wz} = -k_{z1} z - \mu N \cos \gamma + f \sin \omega t \tag{12}$$

In comparison with Eq. (6), in this equation, we need to consider the friction force. Thus, the contact force N should be included, but it is still not obtained. Similar to Eq. (7), from F that is applied force to the gear tooth via the worm screw and F_{Wz}, the normal force N can be obtained as follows.

$$N = F \cos \gamma - F_{Wz} \sin \gamma \tag{13}$$

In this case, if $N = 0$, the teeth are on the verge of losing contact and begin to jump. If Λ is defined as $\Lambda = F_{Wz}/F$, the condition in which the gear teeth begin to jump is obtained.

$$\Lambda = 1/\tan \gamma \tag{14}$$

Next, we consider the force F_r that is parallel to the inclined surface, and obtain the condition in which the teeth of the worm gear begin to slip. The force F_r that is parallel to the lead angle is calculated as follows.

$$F_r = F \sin \gamma + F_{Wz} \cos \gamma - \mu N \tag{15}$$

$$= F(\sin \gamma - \mu \cos \gamma) + F_{Wz}(\cos \gamma + \mu \sin \gamma) \tag{16}$$

We define $\Lambda_r = F_r/F$,

$$\Lambda_r = (\sin \gamma - \mu \cos \gamma) + \Lambda(\cos \gamma + \mu \sin \gamma). \tag{17}$$

In this equation, when $F_r = 0$ or $\Lambda_r = 0$, the worm screw can begin to rotate because of the force applied by the worm wheel. Thus, the condition Λ, where the teeth of the gear begin to slip, is obtained.

$$\Lambda = \frac{\mu \cos \gamma - \sin \gamma}{\cos \gamma + \mu \sin \gamma} \tag{18}$$

Therefore, when the conditions of Eq. (14) or Eq. (18) are satisfied, the worm gear achieves backdrivability.

Now, the condition that is satisfied faster is considered. The specifications of the worm gear are shown in Table 1. Using the lead angle $\gamma = 7.18°$ and the friction coefficient $\mu = 0.175$ in Eqs. (14) and (18), $\Lambda > 7.94$ and $\Lambda > 0.05$ can be obtained respectively. Therefore, when the vibration is added to the axis of the worm wheel W_z, the backdrive is created by the slippage.

Finally, we compare Eqs. (7), (10), (14) and (18). In these equations, Λ is the ratio of the exciting force F_z to the pushing force F between the gear teeth generated by the torque of the worm wheel. Therefore, when the exciting force is added to the axis of the worm wheel, it can be backdriven by a smaller exciting force.

Experiment

Experimental setup

To confirm the above-mentioned theory, we performed experiments.

The experimental setup to vibrate the worm screw axis is shown in Fig. 5. To reduce the worm screw stiffness in the axial direction, the shaft is passed through the linear bushes and supported by the spring. The stiffness of the worm wheel shaft is calculated as a beam supported at both ends. The pulley is attached to the shaft of the worm wheel via a coupling. By hanging a weight to the pulley, a torque can be imparted to the worm wheel.

The experimental setup to vibrate the worm wheel axis is shown in Fig. 6. To reduce the worm screw stiffness in the axial direction, the shaft is passed through the linear bushes and supported by the coupling. In

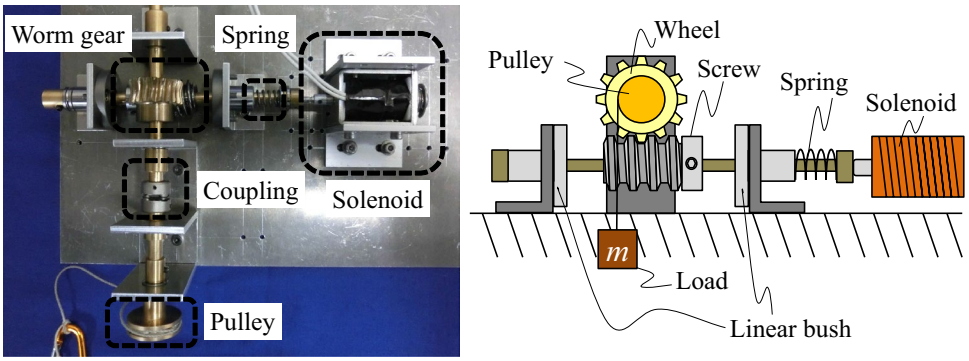

Fig. 5 Experimental setup to observe the backdrivability when the worm screw is vibrated

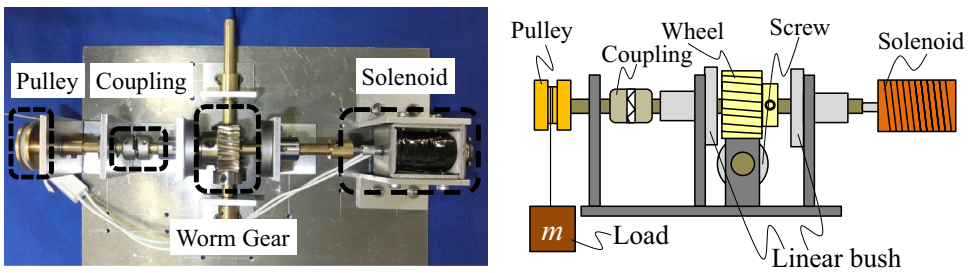

Fig. 6 Experimental setup to observe the backdrivability when the worm wheel is vibrated

this setup, the coupling works as a spring. The pulley is connected to the opposite side of the coupling to impart torque to the worm wheel. The stiffness of the worm screw shaft is calculated as a beam supported at both ends.

In both experiments, a solenoid is used to generate the exciting force. The specifications of the worm gear are shown in Table 1. The weights of the worm gear, including those of the shafts and the stiffness of the shafts, are shown in Table 2. The diameter of the pulley that is attached to the worm wheel shaft is 20 mm, the same as the reference diameter of the worm wheel. Therefore, the hung weight and the force applied to the worm wheel tooth become the same. The pulley is connected to the shaft of the worm wheel via a coupling; thus its weight does not affect M_G.

Measurement of the exciting force

The solenoid used to generate the exciting force generates a counter electromotive force when the direction of the current is changed. If the frequency becomes high, it may not generate enough exciting force. Therefore, we measured the relationship of the voltage, frequency, and exciting force of the solenoid. The experimental setup is shown in Fig. 7. To drive the solenoid, we used a motor driver powered by pulse width modulation (PWM). The shaft of the solenoid is pushed against the center of a both-ends-supported leaf spring. The pushing force is measured by the strain gauge attached to the leaf spring. The strain gauge measures the force as a sine wave, and the maximum value of the force is the exciting force *f*.

While maintaining the arbitrary frequency of the PWM, the voltage is increased in intervals of 5 V from

Table 2 Weight of the worm screw and wheel and spring stiffness of each shaft

Mass	(g)	Worm screw vibration		Worm wheel vibration	
		Spring stiffness	(N/mm)	Spring stiffness	(N/mm)
M_S	59	Worm wheel shaft (bending) k_{y1}	3166.69	Worm wheel axis (compression) k_{z1}	27.88
M_G	70	Worm screw axis (compression) k_{y2}	5.81	Worm screw shaft (bending) k_{z2}	1579.78
		Total (k_{y1}+k_{y2})	3172.50	Total (k_{z1}+k_{z2})	1607.66

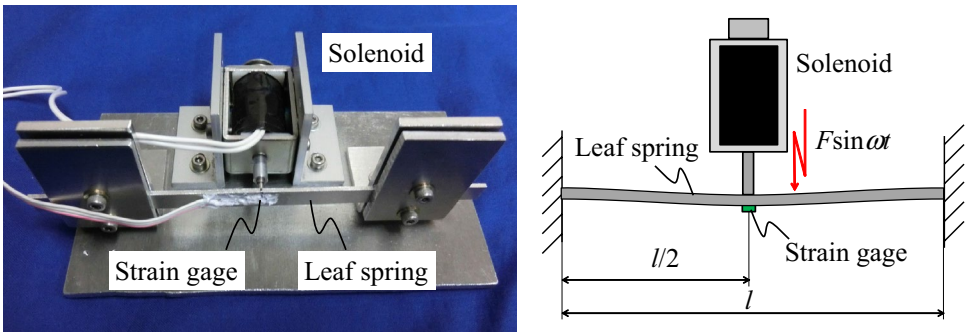

Fig. 7 Experimental setup to measure the pushing force of the solenoid at each frequency

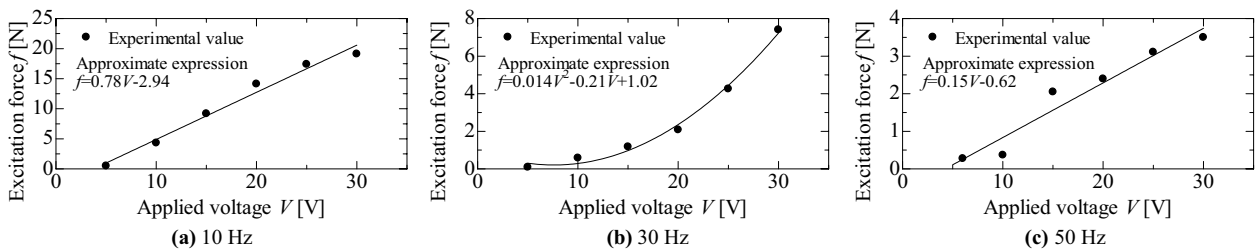

Fig. 8 Relationship between the pushing force and the frequency of the solenoid and their approximate expressions

0 to 30 V, and f is measured. The voltage V and exciting force f are plotted on a graph and their best fit curves are determined. We conducted this experiment at PWM with frequencies of 10, 30, and 50 Hz. The results are shown in Fig. 8. The determined best fit curves are also shown in the graph. Only in the results of the PWM at 30 Hz could linear approximation not be used. However, we used this data for the following experiment. The results show that when the frequency becomes high, the exciting force f of the solenoid becomes small.

Theoretical value of the exciting force for back drive

From the values shown in Table 2 and the conditional expressions shown in the chapter titled "Modeling method of the vibrating worm gear", the required exciting force for achieving backdrivability can be obtained. Figure 9 shows the flow chart for obtaining the theoretical value of the exciting force f_{ref}. The displacement of the vibration is obtained from the motion equation of the whole worm gear mechanism. From the obtained value, the forces applied to the gear (F_{Sy} and F_{Gz}) are calculated. These are then substituted for the conditional expressions to evaluate whether the gear can be backdriven or not. If not, the exciting force is increased to obtain one that satisfies the conditional expressions. At the frequencies of 10, 30, and 50 Hz with the pushing force of the gear teeth F in the range of 1–10 N, we obtained each required exciting force along the worm screw axis and worm wheel axis.

Measurement of the required exciting force for back drive

We measured the required exciting force by the experimental setup shown in Figs. 5 and 6. A weight is hung from the pulley of the worm wheel shaft to apply a pushing force on the worm gear teeth. The solenoid is driven to apply the exciting force to the shaft, and the applied voltage of the solenoid is increased. If the worm gear starts to backdrive, the applied voltage is recorded. From Fig. 8, the exciting force f can be obtained. The procedure is repeated at the frequencies of 10, 30, and 50 Hz with the pushing force of the gear teeth F increased in 1 N steps from 1 to 10 N. The experimental data and theoretical values are shown in Fig. 10.

In the case where the exciting force is applied to the shaft of the worm wheel, the experimental data are well matched to the theoretical values. On the other hand, when the exciting force is applied to the shaft of the worm screw, only some of the experimental values are similar to the theoretical values, thus showing different behavior. In theory, we considered that backdrivability can be obtained when the worm screw and the worm wheel lost their contact. However, in the actual motion, if the gear teeth are separated, the worm screw cannot

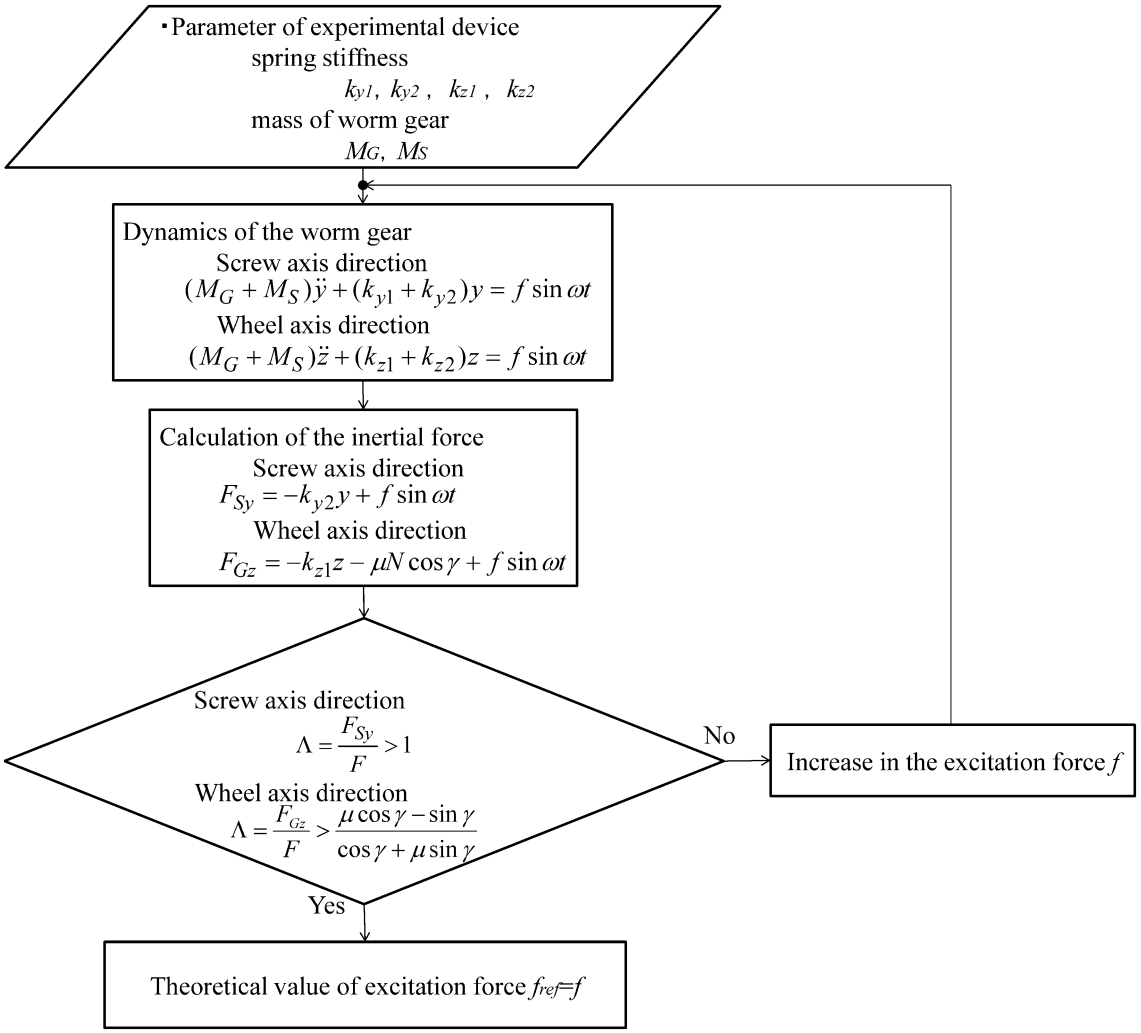

Fig. 9 Flow chart showing the method to obtain the theoretical value of excitation force *f*

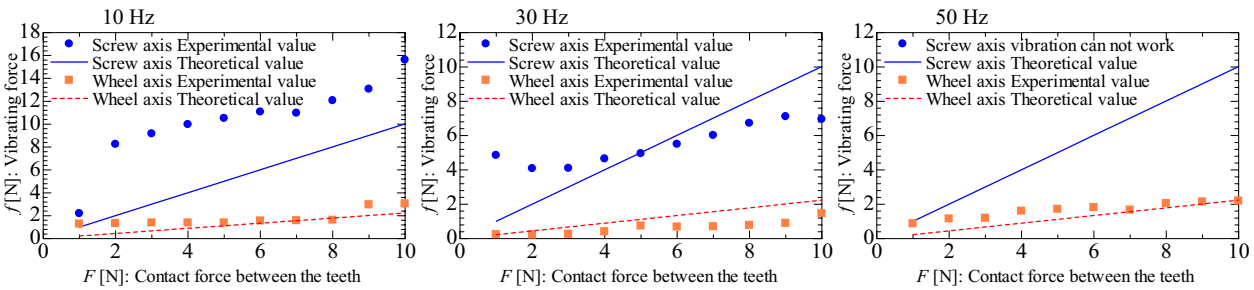

Fig. 10 Vibration force that gives backdrivability to the worm gear mechanism at each contact force between the worm screw and the worm wheel

rotate naturally. When the gear teeth make a collision after the jump, the gear teeth are bounced against other, which rotates the worm screw slightly. Thus, if the height of the jump is large, it bounces several times and it makes backdrivability easy. On the other hand, if the jump is small, the teeth become a single body without bounce.

Therefore, the inclination of the experimental data may be lower than the theoretical data. Moreover, when the frequency is high the worm screw can rotate continuously, but when the frequency is low, the worm screw stops its rotation during its teeth contacting term, and is required to accelerate at every collision. We considered that this is the reason why the required exciting force in the experiment at 10 Hz is larger than the theoretical value. When the exciting force is applied to the shaft of the worm wheel, such discontinuous jumping motion does not occur, and it is well matched to the theoretical value. From these results, we consider that it is better to apply the exciting force to the shaft of the worm wheel.

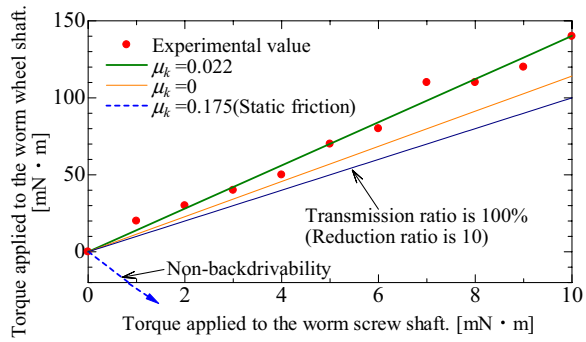

Fig. 11 Torque transmission ratio when the exciting force is applied to the shaft of the worm wheel

Apparent coefficient of dynamic friction and torque transmission ratio

In the former experiment, no torque was applied to the worm screw. However, when the proposed gear mechanism is practically used, torque is applied to the shafts of both the worm screw and the worm wheel. Thus, we attached a pulley to the shaft of the worm screw, applied torque to the shafts of both the worm screw and the worm wheel, and measured the transmission torque when it was backdriven by applying the exciting force to the shaft of the worm wheel. To obtain enough backdrivability, the applied frequency and voltage of the solenoid were 30 Hz and 30 V, respectively. The diameter of the additional pulley attached to the worm screw was 20 mm. The weight hung on the pulley of the worm screw was 0.1 N steps from 0.1 to 1 N. Once weights were hung on both pulleys for balance, the weight hung on the pulley of the worm wheel was increased in 1 N steps, and the weight at which the worm gear started to backdrive was measured. By assuming dynamic friction as μ_k, we obtained the transmission ratio theoretically. F and F_n can be calculated.

$$F = 2T_G/D_G \tag{19}$$

$$F_n = F\cos\alpha\cos\gamma, \tag{20}$$

where T_G and D_G are the applied torque to the worm wheel and the reference diameter of the worm wheel, respectively. Thus, the transmit torque from the worm screw to the worm wheel can be obtained.

$$T_S = \frac{F_n D_S}{2}(\cos\alpha\sin\gamma - \mu_k\cos\gamma), \tag{21}$$

where D_S is the reference diameter of the worm screw. We obtained the apparent coefficient of dynamic friction from the experimental results, as shown in Fig. 11. The theoretical values in the cases of the coefficient of dynamic friction are 0.175 (the same as the coefficient of static friction) and 0, as shown in the graph. A line is also shown that indicates the transmission ratio, calculated from the gear ratio of 10, is 100 %. We can confirm that when $\mu_k = 0.175$ it cannot be backdriven, and the transmission ratio of the experimental values are less than the theoretical value of $\mu_k = 0$. From the results, we can obtain the apparent coefficient of dynamic friction as 0.022, and its torque transmission ratio is 71 %.

Discussion and conclusion

In comparing the exciting forces applied along the worm screw axis and worm wheel axis, the force applied to the worm screw was found to be larger. This result was the same as the theoretical result. The experimental results and theoretical results when the exciting force was applied to the worm wheel were well matched. Regretfully, the behaviors of the experimental results and theoretical results when the exciting force was applied to the worm screw axis were different. We considered that the difference was due to the discontinuous jumping of the gear teeth. In the range of the conducted experiment, when the exciting force was applied to the worm wheel axis at the frequency of 30 Hz, it could be backdriven by the smallest exciting force.

From the theoretical equation, we considered that the backdrivability was not influenced by the vibration frequency. However, the experimental results when the exciting force was applied to the worm screw axis demonstrated that if the frequency was low, the required exciting force is increased. Moreover, if the frequency become high, the solenoid could not generate sufficient exciting force. Therefore, in the future, we intend to use actuators that can apply a large exciting force with high frequency (such as a piezo actuator) to extend the experimental range. In this paper, we only focused on the required exciting force that the worm gear could obtain for backdrivability. Moreover, in the experiment, we observed not only that the weight hung on the pulley

attached to the worm wheel shaft could start to drop by applying the exciting force to the worm gear, but also that the weight sometimes did not accelerate and drop at a constant velocity. This means that to predict the behavior during backdriving, we need to create another dynamic model that includes a viscosity effect. We consider this to be another future work.

Acknowledgements
Not applicable.

Authors' contributions
TT contributes to propose the basic idea and design the experimental systems. NH contributes to develop the experimental systems and conduct the experiments. Both authors read and approved the final manuscript.

Funding
Not applicable.

Availability of data and materials
The datasets used and/or analyzed during the current study are available from the corresponding author on reasonable request.

Competing interests
The authors declare that they have no competing interests.

Received: 27 September 2019 Accepted: 5 December 2019
Published online: 19 December 2019

References

1. Albu-Schaffer A, Eiberger O, Grebenstein M, Haddadin S, Ott C, Wimbock T, Wolf S, Hirzinger G (2008) Soft robotics. IEEE Robot Autom Mag 15(3):20–30
2. Kai Y, Sando S (2014) Development of a velocity and contact force-based mechanical safety device for service robots. In: 2014 IEEE international conference on automation science and engineering (CASE), IEEE, pp 1188–1193
3. Laurin-Kovitz KF, Colgate JE, Carnes SD (1991) Design of components for programmable passive impedance. In: Proceedings, 1991 IEEE international conference on robotics and automation, IEEE, pp 1476–1481
4. Bicchi A, Tonietti G (2004) Fast and soft-arm tactics [robot arm design]. IEEE Robot Autom Mag 11(2):22–33
5. Wang L, Iida F (2015) Deformation in soft-matter robotics: a categorization and quantitative characterization. IEEE Robot Autom Mag 22(3):125–139
6. Kawasaki H, Murakami S, Kachi H, Ueki S (2008) Novel climbing method of pruning robot. In: 2008 SICE annual conference, IEEE, pp 160–163
7. Yeh T-J, Wu F-K (2005) Modeling and robust control of worm-gear driven systems. In: IEEE international conference on mechatronics, ICM'05, IEEE, pp 711–716
8. Kong K, Bae J, Tomizuka M (2011) A compact rotary series elastic actuator for human assistive systems. IEEE/ASME Trans Mechatron 17(2):288–297
9. Takayama T, Yamana T, Omata T (2010) Three-fingered eight-dof hand that exerts 100-n grasping force with force-magnification drive. IEEE/ASME Trans Mechatron 17(2):218–227
10. Takayama T, Arakawa T, Omata T (2012) Coupled driven variable transmission unit. Trans Jpn Soc Mech Eng 78(794):3541–3551 **(in japanese)**
11. Iwamoto T, Itai Y, Shiroyama K, Nagano A (2009) Realization of pseudo mechanism function using a worm gear. J Robot Soc Jpn 27(10):1154–1159 **(in japanese)**
12. Tadakuma R, Tadakuma K, Takagi M, Onishi S, Matsui G, Ioka K, Tsumaki Y, Higashimori M, Kaneko M (2013) The gear mechanism with passive rollers: the input mechanism to drive the omnidirectional gear and worm gearing. In: 2013 IEEE international conference on robotics and automation, IEEE, pp 1520–1527
13. Godfrey D (1967) Vibration reduces metal to metal contact and causes an apparent reduction in friction. ASLE Trans 10(2):183–192
14. Yokoyama Y (1971) Friction reduction effect by the vibration. J Jpn Soc Mech Eng 74(630):805–813 **(in japanese)**
15. Hisamatsu N, Takayama T, Omata T (2013) Worm gear that can change its backdrivability. In: JSME conference on robotics and mechatronics, JSME, pp 2–103 **(in japanese)**
16. Takayama T, Hisamatsu N, Omata T (2014) Worm gear that can change its backdrivability-2nd report the influence that vibration direction gives in backdrivability-. In: JSME conference on robotics and mechatronics, JSME, pp 2–205 **(in japanese)**

Publisher's Note